Flow structures and drag characteristics of a colony-type emergent roughness model mounted on a flat plate in uniform flow

Takeshi Takemura[a] and Norio Tanaka[b,*]

[a]Graduate School of Science and Engineering, Saitama University,
255 Shimo-okubo, Sakura-ku, Saitama-shi, Saitama-ken 338-8570, Japan

[b]Faculty of Engineering, Saitama University,
255 Shimo-okubo, Sakura-ku, Saitama-shi, Saitama-ken 338-8570, Japan

Received 25 November 2004;
revised 2 June 2006;
accepted 1 June 2007
Communicated by S. Kida

Abstract

The characteristics of flow structures around a colony-type emergent roughness model, hereafter called 'colony model', mounted on a flat plate in uniform flow and the drag coefficient C_{dc} for the colony model are investigated by flow visualization, spectral analysis, velocity measurement and drag force measurement. Two types of colony models, each comprising seven equally spaced cylinders with grid or staggered arrangement are mounted on a water flume bed. The flow structure around the colony model changes depending on L/D and G/D (L: space between neighboring cylinders, D: diameter of a cylinder, G: space between cylinders in the cross-stream direction). Two types of flow structures, a large-scale Kármán vortex street (LKV) behind the colony models and a primitive Kármán vortex street (PKV) behind the individual cylinders, are generated. LKV is formed along the shear layer for $G/D < 0.4$. When $G/D > 1.8$, PKV behind each cylinder is stably formed because of the decrease in difference between the velocity through the colony model and that of the detour flow. The velocity through the colony model, which plays a key role for the phenomenon change, strongly increases with G/D at first and then gradually. The tendency of the velocity curve changes around $G/D = 1.8$ for each arrangement. It almost coincides with the initiation of the formation of PKV. On the other hand, C_{dc} for the colony model increases in the range of $0.08 < G/D < 0.75$ ($0.25 < L/D < 1$) and $0 < G/D < 1$ ($1 < L/D < 3$) for the grid and staggered arrangements, respectively. The changing point of the tendency in the C_{dc} curve is located in the middle of the transition zone for the two vortex structures ($0.4 < G/D < 1.8$). Moreover, the C_{dc} value for the colony model is nearly constant, independent of the two arrangements, when $G/D > 1.8$.

Key words: Colony type vegetation, Drag coefficient, Strouhal number, Flow structure, Grid or staggered arrangement, Flow visualization, PIV

*Corresponding author. Tel.: +81 48 858 3564; Fax: +81 48 858 3564

E-mail address: n-tanaka@post.saitama-u.ac.jp (N. Tanaka)

1. Introduction

The effects of vegetation on resistance to river flow, such as flow discharge and water depth have become one of the major interests of river engineers, and many experiments in water flume and numerical analyses have been conducted (Kouwen *et al.*, 1981; Helmiö, 2002; Järvelä, 2002; Righetti and Armanini, 2002; Struve *et al.*, 2003; Choi and Kang, 2004). The effects of density and vegetation characteristics on the changes of drag force to flow are also important for evaluating bulk roughness characteristics (Nepf, 1999).

In many previous studies, circular cylinders were substituted for vegetation and arranged in a grid or staggered in a water flume (Smith *et al.*, 1990; Okamoto *et al.*, 1994; Musick *et al.*, 1996). Li and Shen (1973) analyzed the flow characteristics considering the multicylinder arrangement (staggered or parallel pattern) and spacing between the cylinders, L/D (L: cross-stream space between neighboring cylinder, D: diameter of a cylinder), and reported the dependence of drag coefficient C_d on L/D. Nepf (1999) investigated the turbulence intensity and bulk drag coefficient of vegetation in different arrangements using experimental data and gave the bulk drag coefficient as a function of vegetation density. Many other studies also demonstrated the importance of L/D, vegetation density and the arrangement of cylinders for evaluation of C_d (Thompson and Roberson, 1976; Okamoto *et al.*, 1994).

A colony-type roughness, rather than a grid-type roughness, is sometimes observed in the initial growth stage of trees (Järvelä, 2002), undershrubs or grasses in a river. Large amounts of sand accumulate behind the colony-type vegetation, such as a willow tree or bushes, on a floodplain or a sand bar, especially when the flood discharge is decreased. As the sand accumulation accelerates the vegetation growth at the habitat, the shallow flow structure around a colony-type vegetation should be elucidated. Only a few studies have been conducted on the colony-type roughness except for the experiments using a group of circular cylinders (Musick *et al.*, 1996) and a perforated plate modeled for submerged silva (Castro, 1971). The drag coefficient increases with increasing porosity of the perforated plate (Castro, 1971). However, many aspects of the flow structures around colony-type roughness remain unclear.

The local flow structures around colony-type emergent vegetation were assumed to be similar to the flow phenomena observed around a single circular cylinder in previous research (Baker, 1980; Okamoto and Yagita, 1973; Okamoto and Sunabashiri, 1992). However, the mutual interference of many cylinders (Zdravkovich, 1977; Tatsuno *et al.*, 1998; Akilli *et al.*, 2004) produces a flow structure significantly different from that of a single cylinder. Dalton and Szabo (1977) investigated the interaction between two or three cylinders aligned in longitudinal direction (Figs. 1a, 1b). In the case of two or three cylinders, C_{ds} at the end position (DST2 and DS3, in Figs. 1a and 1b), is smaller than that at the front (DST1 and DS1). In the range of $L/D < 2$, C_{ds} at the back position of three cylinders (DS3) is smaller than that for the two cylinders (DST2) because of the velocity difference in approach flow to the back cylinder. However, when the cylinder at the back is located outside the reattachment point of the front cylinder (i.e., L/D is larger than approximately 4), the drag force acting on the back cylinder in the second row (DST2) is smaller than that in the third row (DS3), indicating the importance of whether the spacing is within the distance between the cylinder and the

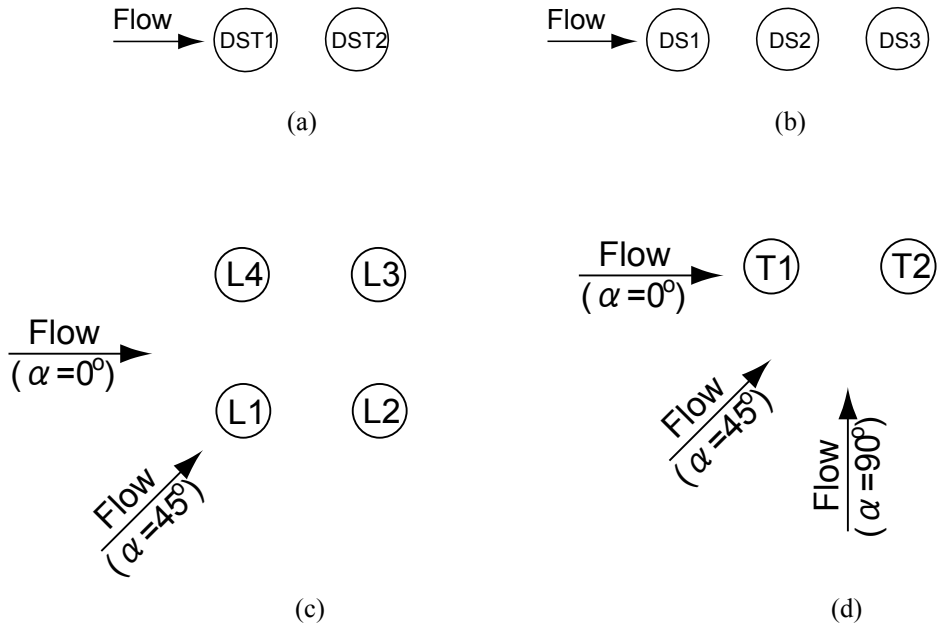

Fig. 1. Arrangements of roughness. (a), (b) Re = 2.78×10^4-7.82×10^4 and l_C/D (l_C: length of cylinder, D: diameter of cylinder)=16 (Dalton and Szabo, 1977), (c) Re=2.25×10^4-5.18×10^4, l_C/D =17 (Lam *et al.*, 2003b), (d) Re=6.2×10^4, l_C/D =20 (Tatsuno *et al.*, 1991).

reattachment point. Sumner *et al.* (1999) reported that the flow pattern around two cylinders changes depending on L/D and that the dependency on the Reynolds number Re (=UD/ν, U: reference velocity (m/s), D: cylinder diameter as a reference length (m), ν:kinematic viscosity (m^2/s) of a fluid) is weak for the range of Re from 500 to 3000.

Four cylinders arranged in a square were studied by Lam *et al.* (2003a, 2003b) (see Fig. 1c). The drag coefficient with different approach angles α to the roughness was measured for each cylinder, indicating the importance of the flow interaction between neighboring cylinders. The importance was also demonstrated by an experiment of Tatsuno *et al.* (1991) (Fig. 1d).

The effects of the ratio of cylinder height and diameter (l_c/D, l_c: cylinder height) on C_{ds} were discussed by Okamoto and Yagita (1973), and many studies were conducted with a high l_c/D. However, it is difficult to apply the results of these past studies to evaluate the roughness characteristics of colony-type vegetation in which low water depth affects the sedimentation process at a flood event. For example, l_c/D is less than 10 when the tree trunk diameters of the colony are about 0.05 m and water depth is less than 0.5 m. As indicated by Melville and

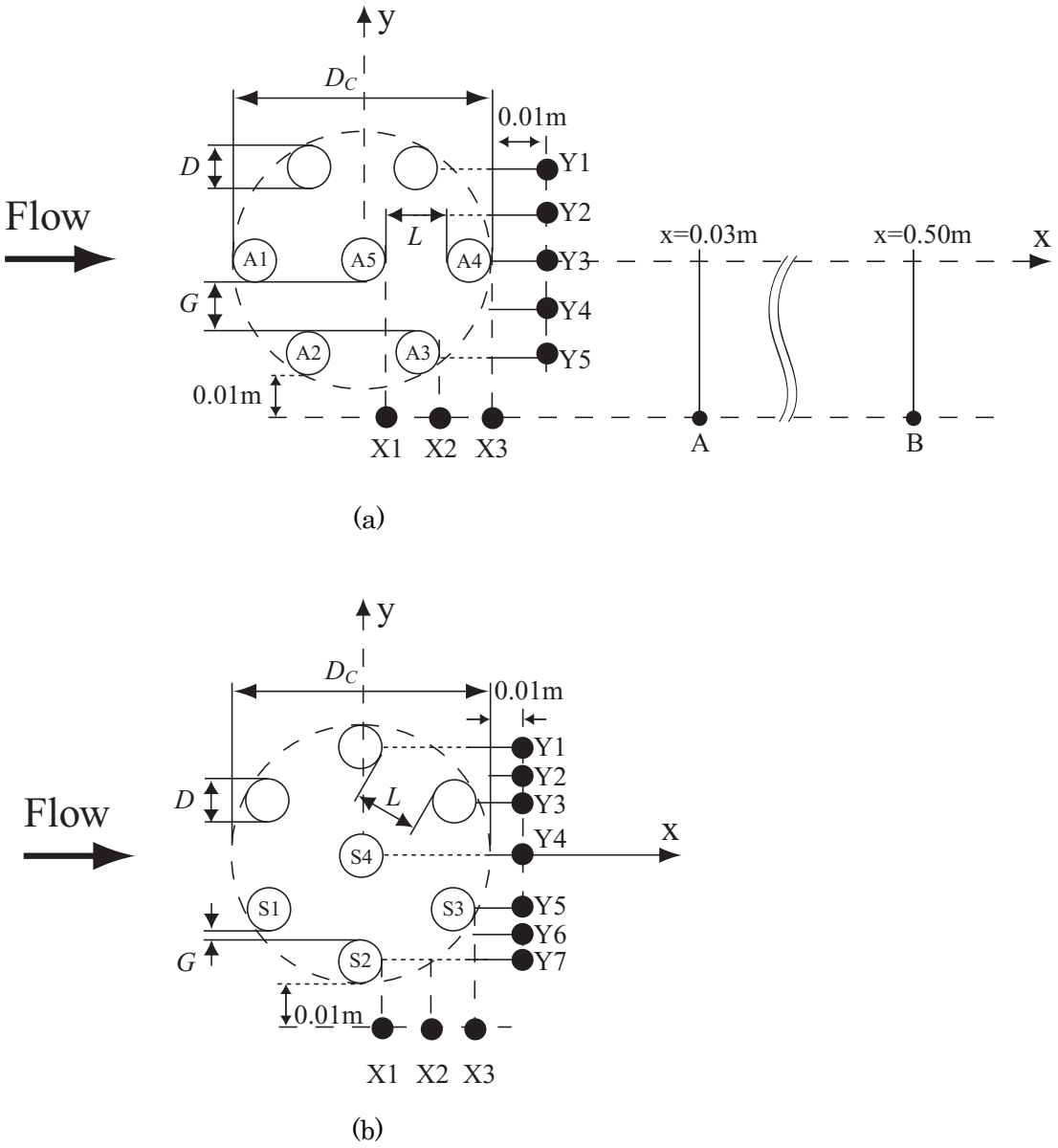

Fig. 2. Definition of the colony model and measurement points of velocity. *D*: Diameter of cylinder, *L*: spacing of each cylinder, *Dc*: outer diameter of the colony model, *G*: spacing of each cylinder in cross-stream direction, the number inside the cylinder, e.g., A1, distinguishes each cylinder's position. (a) grid arrangement, (b) staggered arrangement. The velocity of the detour flow past the colony model and the velocity through the colony model are measured at points indicated by closed circles (X1-X3 and Y1-Y7).

Sutherland (1988), local scour depth around bridge piers varies for the water depth and cylinder diameter ratio, H/D (H: water depth, $H=l_c$ when the roughness is in emergent condition.) of about 3 but not much around 3-7. Therefore, the present study focuses on the effect of spacing (L/D) on cylinders arranged like a colony with a low H/D = 5.

Table 1 Experimental conditions

Spacing of adjacent cylinders (L) / Diameter of each cylinder (D) (L/D)	Spacing of each cylinder in cross-stream direction (G) / Diameter of each cylinder (D) (G/D)		Mean velocity (U) (m/s)					
			0.04		0.1		0.4	
	grid	staggered	grid	staggered	grid	staggered	grid	staggered
0.25	0.1	-0.4	-	-	g	-	d	d
0.5	0.3	-0.3	g	-	g	g	c	c
1	0.7	0	g	-	g	g	e	d
2	1.6	0.5	-	-	g	-	a	f
3	2.5	1	g	-	g	g	c	d
5	4.2	2	g	-	g	-	d	f

a : measurement of drag coefficient on colony model (C_{dc}) and on each cylinder (C_{ds})
b : measurement of drag coefficient on colony model (C_{dc}), flow visualization and frequency analysis
c : measurement of drag coefficient on colony model (C_{dc}) and on each cylinder (C_{ds}), flow visualization and frequency analysis
d : measurement of drag coefficient on colony model (C_{dc}) and flow visualization
e : measurement of drag coefficient on colony model (C_{dc}) and on each cylinder (C_{ds}) and flow visualization
f : measurement of drag coefficient on colony model (C_{dc})
g : flow visualization
- : unmeasured

To elucidate the flow structures, we conduct flow visualization, velocity distribution measurement, spectral analysis and drag-force measurement, paying special attention to the flow structures in front of the obstacle and in the wake (Tamai *et al.*, 1987).

2. Experimental arrangement and procedures

2.1. Experimental apparatus

Laboratory experiments are conducted in a water flume (bed slope gradient range: 0~1/50, maximum discharge: 0.1 m^3/s) that is 15 m in length and 0.5 m in width. The colony model is mounted on the water-flume bed at 8.5 m from the upstream inlet and in the center in a cross-stream direction. The mean flow velocity U in the flow cross-sectional area normal to the streamwise direction of the open channel flow is set at 0.04, 0.1 and 0.4 m/s for L/D=0.25, 0.5, 1, 2, 3 and 5 (D = 1 cm). The corresponding Reynolds number based on the diameter of a single cylinder and the mean velocity of approach flow ranges from 400 to 4000. The experiments are carried out with a fixed 1/1000 bed slope and 0.05 m water depth. The flow discharge is controlled by a valve and gate system at the end of the water flume. The bed slope and water surface gradient from the section 2 m upstream of the roughness to the section 4 m downstream are confirmed to be almost the same by point gage measurements.

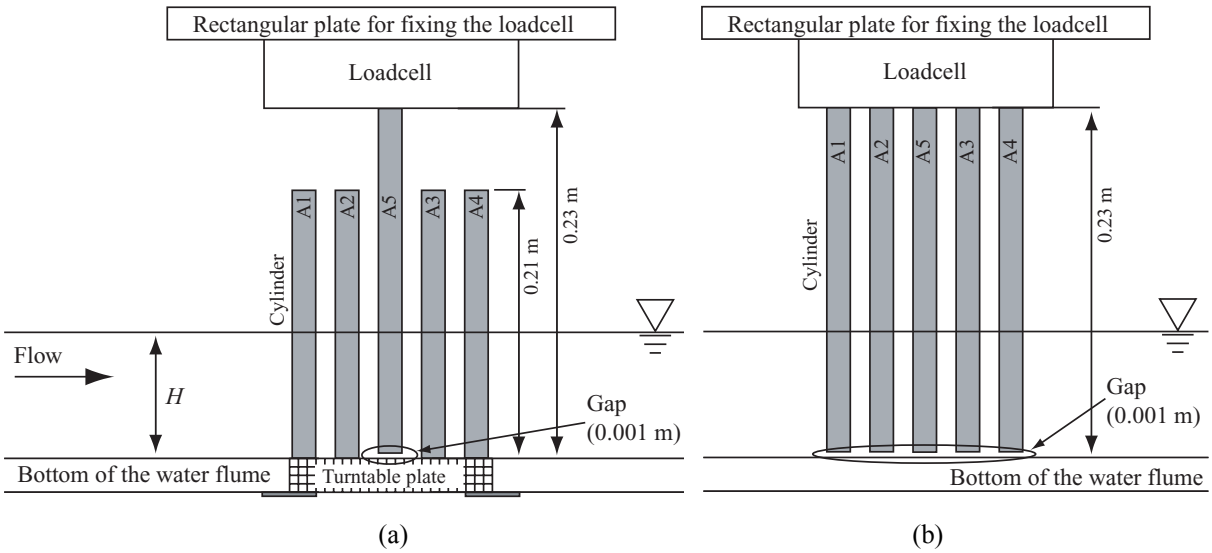

Fig. 3. Schematic of the colony model and load cell mounted in the water flume. (a) measurement of drag force on a cylinder, (b) measurement of drag force on the colony model.

2.2. Colony model

The drag forces on two or three cylinders with different positions were investigated in previous studies (Dalton and Szabo, 1977; Kiya *et al.*, 1980; Kim and Durbin, 1988; Tatsuno *et al.*, 1991), but a larger number of cylinders should be investigated to elucidate the drag force on colony-type vegetation. In the present study, the colony model includes three types of alignments, i.e. two cylinders in a longitudinal direction, three cylinders in a longitudinal direction and two cylinders in a cross-stream direction. The colony model is made of seven wood cylinders, which are placed equidistantly at the vertices of a hexagon and at the center (Fig. 2). The weights of the colony model and individual cylinders for drag measurement are around 125 g and 53 g, respectively, independent of L/D. The experiments are conducted in grid and staggered arrangements (see Figs. 2a, 2b). Free damping oscillation experiments show that the undamped natural frequency of the colony model is between 11.8 - 12.6 Hz in air and 8.3 - 9.3 Hz in water, and damping ratio, logarithmic decrement rate of amplitude, of the colony model is 1 % in air. The experimental conditions (Table 1) are chosen to make comparison with the previous roughness type shown in Figs.1(a)-(d) (Dalton and Szabo, 1977; Tatsuno *et al.*, 1991; Lam *et al.*, 2003a, 2003b).

Considering the importance of the space between neighboring cylinders and the distance between a cylinder and the reattachment point of the wake (Dalton and Szabo, 1977), we set the experimental condition so that the upper limit of L/D is 5.

2.3. Drag force and velocity measurement

A two-axis load cell (streamwise (X) and transverse (Y) directions, type LB-60, SSK Co., Ltd.) that has a resolution of 1/1000 and can measure 1 N for the maximum load is used to

measure the drag force on the colony model. A schematic of the cylinder locations in the water flume is shown in Fig. 3.

Aniline blue is used to visualize the flow around the colony model at three velocities, 0.04, 0.1 and 0.4 m/s. The images are recorded directly on a PC by using a 3CCD digital video camera (Panasonic Co. Ltd.; NV-GS100K; 720 pixels × 480 pixels, 30 fps). Vortex shedding frequencies are counted using 20 different sets of time series data of visualized flow patterns with 30 seconds in each. Velocity is measured by an electromagnetic flow meter (type of main amplifier: VM-2000, type of sensor: VMT2-200-04P, KENEK Co., Ltd.; the sensor is 15 mm in length and 4 mm in diameter, and the measurement point is located at the middle height of the sensor), with 30-second and 100 Hz sampling frequencies. The water velocities through the colony model are measured at the points marked with black circles in Fig. 2. The mean flow velocity U is obtained by averaging velocities at 36 points of a cross-section (9 for the cross-stream direction every 50 mm between 50 and 450 mm points and 4 for the vertical direction every 10 mm between 10 and 40 mm from the water flume bed). The water velocity calculated from the discharge measurement by a triangular weir and that calculated by an electromagnetic flow meter have a difference of only 2 %. The water velocity field around the colony model is measured by a PIV system. Flow visualization is carried out using a 50 mW green-laser sheet (YAG/YVO_4 laser) and aluminum powder. The turbulence intensity, $\sqrt{\overline{u'^2}}/U$ (u' being the fluctuation velocity in the streamwise direction), measured by the PIV method in a vertical direction takes 0.5-1.2 % from the bed to the water surface. The mean water velocity analyzed by the PIV system and that calculated by the electromagnetic flow meter agree within 3 %. The power spectrum of the drag force and the velocity fluctuation through the colony model in direction Y at points A and B (Fig. 2) are analyzed by using the maximum entropy method.

The drag coefficients and Strouhal numbers (denoted by C_{dc} and S_{tsh} for the colony model, C_{ds} and S_{tg} for each solid circular cylinder) are defined by

$$C_{dc} = \frac{2F_c}{\rho U^2 A_P}, \quad C_{ds} = \frac{2F_s}{\rho U^2 DH}, \tag{1}$$

$$S_{tsh} = \frac{f_s D_c}{U} \ , \ S_{tg} = \frac{f_g D}{U} \tag{2}$$

Here, F_c (N) is the total drag force on solid circular cylinders in the colony model, and F_s (N) is the drag force on each solid circular cylinder. ρ (kg/m^3) is the fluid density. A_P (m^2) is the frontal projection area (i.e. the number of visible solid circular cylinders in the colony model from upstream $\times D \times H$). f_g (Hz) is the shedding frequency from each circular cylinder. f_s (Hz) is that of the generated vortices from the colony model and D_c (m) is the outer diameter of the colony model.

For measuring the drag force, a gap is required between a cylinder or the colony model and the flume bottom. The influences of the gap on drag coefficient are investigated by changing the gap distance from the water flume bed. Gaps of 0.002 m and 0.006 m

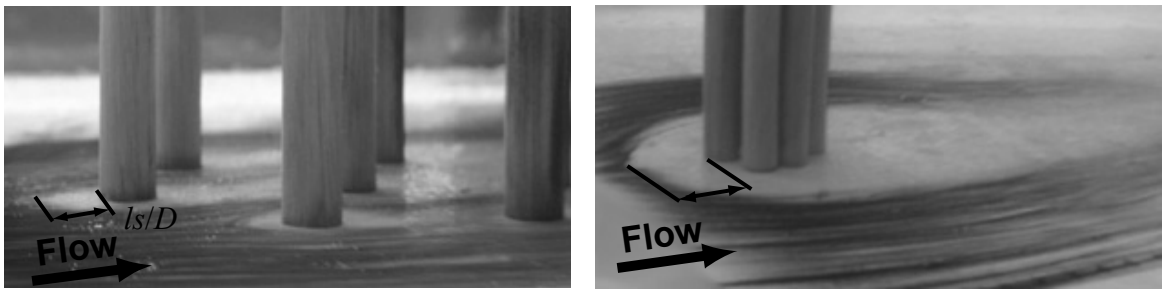

(a) (b)

Fig. 4. Visualized flow pattern around the colony model with a grid arrangement for U = 0.4 m/s. (a) L/D = 3, (b) L/D = 0.5. The arrow shows the flow direction. l_s: the width of the separation zone in front of the A1 cylinder.

cause 2% and 9% losses of drag force, respectively, compared with a gap of 0.001 m. The experiments are conducted with the smallest possible gap, 0.001 m, for the measurement of drag forces. With this gap, the separation line in front of the colony model is not different from the no gap case, as explained in the following section.

3. Results

3.1. Flow structures around the colony model

Flow structures in front of the colony model with a grid arrangement are different depending on L/D (Fig. 4). Not horseshoe vortices around the cylinders but separation zones appear because the dye at bottom is removed by the horseshoe vortices. A separation zone around the colony model is observed for L/D = 0.5, while small separation zones around each cylinder are generated by horseshoe vortices for L/D > 2. When the mean velocity increases from 0.1 to 0.4 m/s (Re = 1.0×10^3 - 4.0×10^3), the non-dimensional length for the separation line, ls/D (see Fig. 4), increases from 0.6 to 0.8 for L/D = 0.25-0.5, while it increases only from 0.15 to 0.2 with the same velocity conditions for L/D = 2-3.

Behind the colony model, on the other hand, three types of vortices are generated depending on L/D for both arrangements (Fig. 5), which is similar to the results by Sayers (1990). In the grid arrangement (Figs. 5a-5d), small separate vortices, hereafter called 'small vortices (SV)', are formed behind the A3 cylinder for L/D = 0.5 (Fig. 5a) along the shear layer. Downstream of SV, a large-scale vortex street, hereafter called 'large-scale Kármán vortex street (LKV)', is formed (Figs. 5a and 5b). When L/D = 1, SV are not generated behind the A3 cylinder. For L/D = 3, a primitive Kármán vortex street (PKV) behind each cylinder (A3 and A4) is generated (Figs. 5c and 5d), but LKV is not clearly formed downstream of PKV. In the staggered arrangement (Figs. 5e and 5f), LKV is also generated clearly for L/D = 0.5. However, for L/D = 3, PKV behind each cylinder is not clearly formed compared with the grid arrangement.

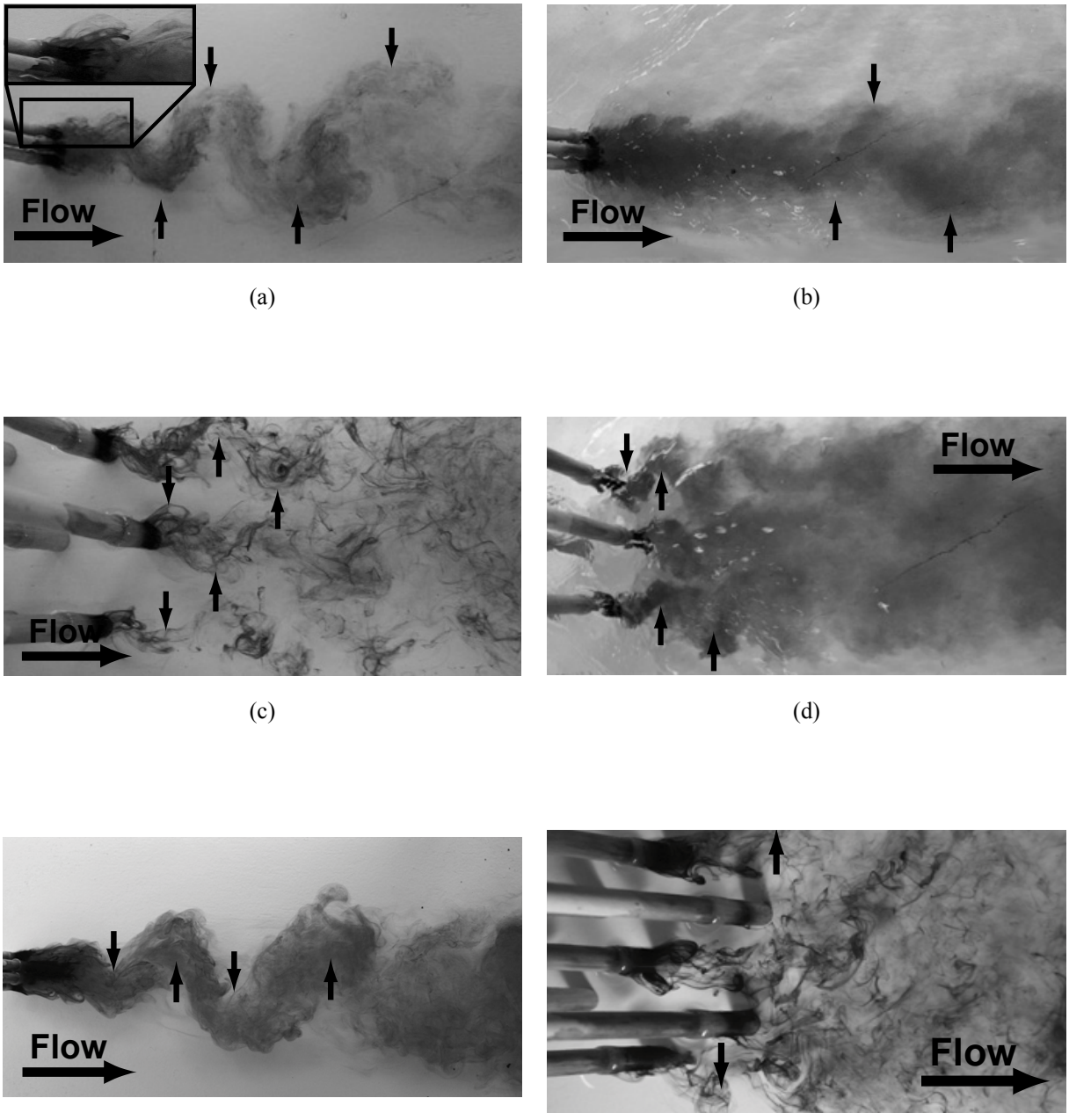

(a) (b)

(c) (d)

(e) (f)

Fig. 5. Flow pattern in the wake of the colony model. (a) L/D=0.5, grid arrangement (Re=400; the zoom photograph is inserted at the upper left corner, (b) L/D=0.5, grid arrangement (Re=4000), (c) L/D=3, grid arrangement (Re=400), (d) L/D=3, grid arrangement (Re=4000), (e) L/D=0.5, staggered arrangement (Re=400) and (f) L/D=3, staggered arrangement (Re=400). The small arrows show the positions of LKV ((a), (b) and (e)) or PKV ((c), (d) and (f)) behind the colony model.

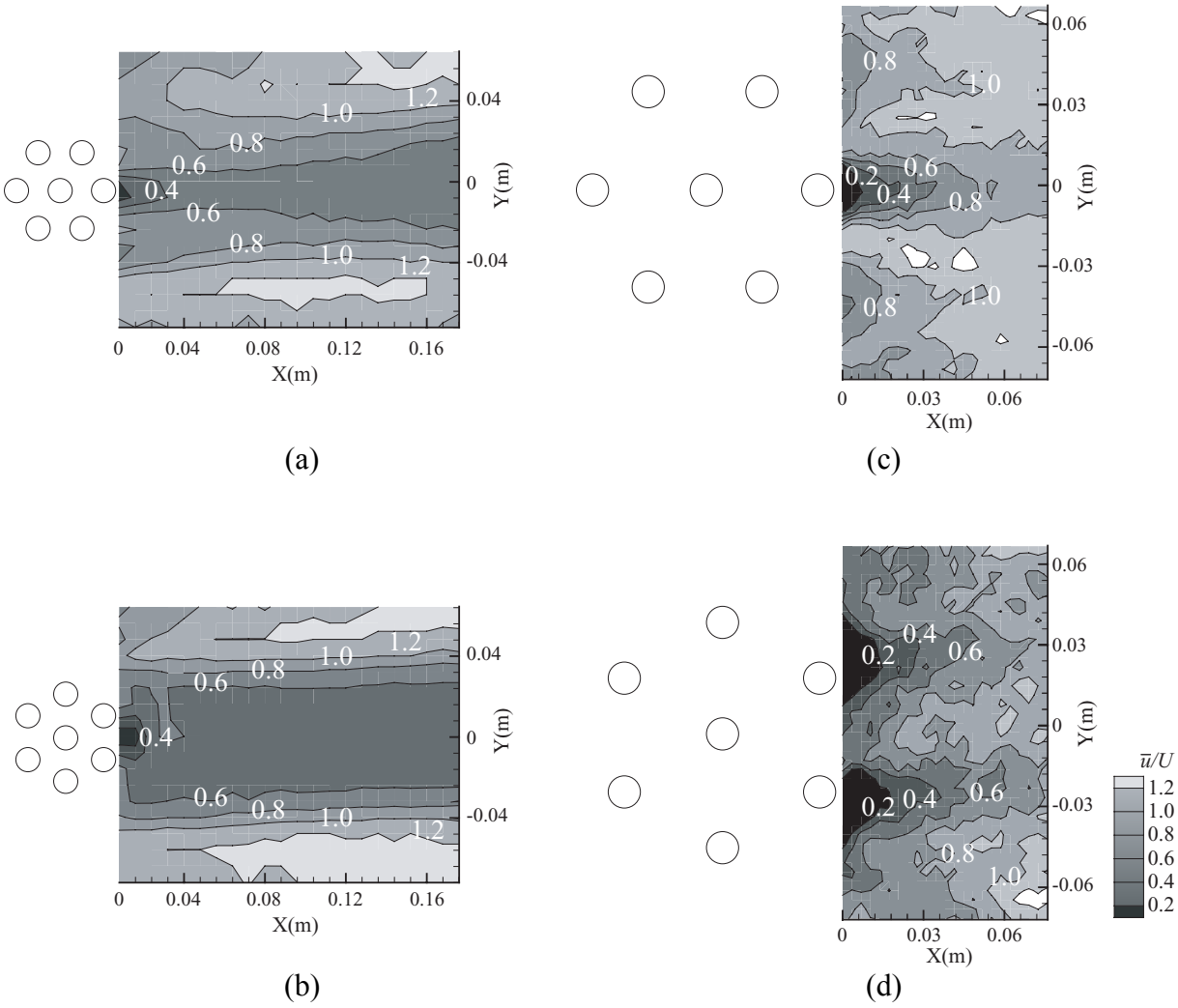

Fig. 6. Non-dimensionalized mean velocity ($\overline{u}/U$) in the streamwise direction contour map is shown behind the colony model, U=0.4 m/s. (a) L/D=0.5 in grid arrangement, (b) L/D=0.5 in staggered arrangement, (c) L/D=3 in grid arrangement and (d) L/D=3 in staggered arrangement.

The differences in streamwise mean velocity $\overline{u}$ behind the colony model in the two Kármán vortex streets, LKV and PKV, are analyzed by non-dimensionalizing $\overline{u}$ with U for the cases of L/D =0.5 and 3, as shown in Fig. 6.

In the grid and staggered arrangements with L/D = 0.5, a slow velocity field ($\overline{u}/U < 0.6$) is observed in a large area with long distance only behind cylinder A4 (Fig. 6a) and behind the model (Fig. 6b).

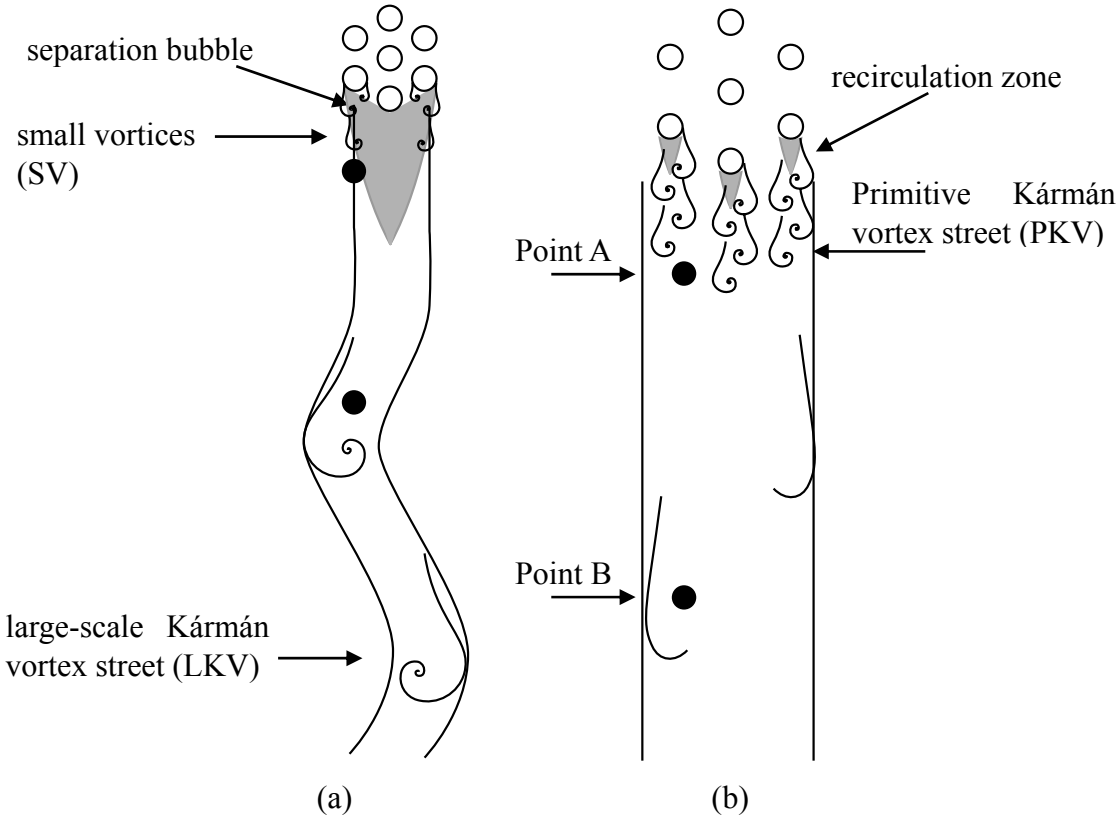

Fig. 7. The schematic of the flow structures behind the colony model with a grid arrangement. (a) L/D=0.5 and (b) L/D=3. The hatched areas show the recirculation zones or separation bubble (for Points A and B, see Fig. 2).

In the grid arrangement with L/D = 3, the slow velocity field is observed in a small area only behind cylinder A4 (Fig. 6c). In the staggered arrangement with L/D =3, the slow velocity fields are observed in small area behind the individual cylinders in the back side of the colony model and these small velocity fields are not separated from each other (Fig. 6d). The schematic of the flow structures behind the colony model is shown in Fig. 7.

3.2. Strouhal number of visualized vortices shed behind cylinders

The Strouhal number is calculated for twelve cases (L/D = 0.5, 1, 3 and U = 0.1, 0.4 m/s for two arrangements) and six cases (L/D = 0.5 and U = 0.04, 0.1, 0.4 m/s for two arrangements) to elucidate the vortex shedding characteristics. Fig. 8 shows the relationships between Strouhal number and Reynolds number with different arrangements and L/D. This figure also includes the data of previous results for a hemisphere on a flat plate (Tamai *et al.*, 1987), where the reference length is the height of the hemisphere. When L/D = 0.5 and 1, S_{tg} is calculated based on the vortices shedding from individual cylinders (PKV or SV in grid and staggered arrangements, A3 and S2), and S_{tsh} is calculated for LKV.

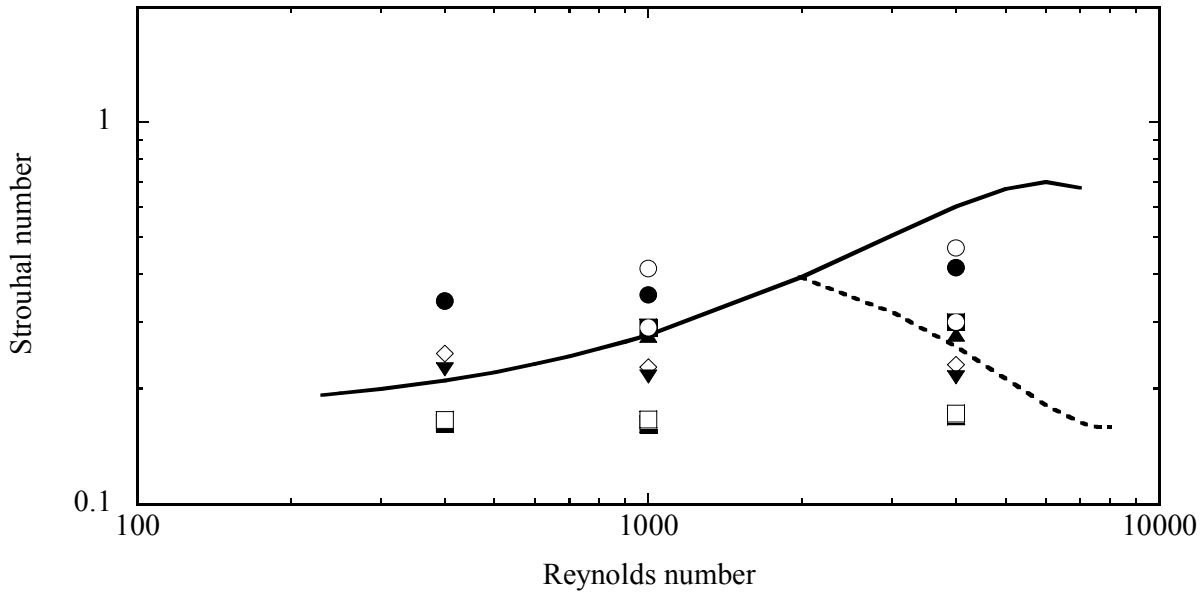

Fig. 8. Strouhal numbers, S_{tg} and S_{tsh}, for vortices from the colony model; solid line, S_{tg}, Hemisphere (Tamai *et al*., 1987); dashed line, S_{tsh}, Hemisphere (Tamai *et al.*, 1987); ●, L/D=0.5 (S_{tg}, grid); ○, L/D=0.5 (S_{tg}, staggered); ■, L/D=0.5 (S_{tsh}, grid); □, L/D=0.5 (S_{tsh}, staggered); ▲, L/D=1 (S_{tg}, grid); ◘, L/D=1 (S_{tg}, staggered); ▼, L/D=3 (S_{tg}, grid); ◊, L/D=3 (S_{tg}, staggered).

To calculate the Strouhal number, the mean velocity in approach flow is used, but this affects the decrease in S_{tsh} for LKV because the velocity through the colony model is smaller than the approach flow velocity. The results in Figs. 5 and 8 indicate that the flow and vortex patterns change depending on L/D rather than the Reynolds number, and this is similar to the results of Sumner *et al.* (1999). The variation of S_{tg} with L/D is discussed in section 4.1.

There are significant variations in S_{tg} with L/D but not between the two arrangements. Thus, to validate the visualized shedding frequencies, spectral analyses are applied for velocities in grid arrangement cases. The power spectral density of velocities with respect to the frequencies of fluctuation at points A and B (Fig. 2) are shown in Figs. 9(a) and (b), respectively. At point A, the characteristics of the spectrum change greatly with L/D (Fig. 9a). There are two peaks around 7.8 Hz and 15.5 Hz when L/D = 3 and 0.5, respectively. These peak frequencies appear in similar ranges to the visualized shedding frequencies of PKV and SV, 8.5 ± 1.2 Hz and 16.7 ± 1.5 Hz. At point B, there is a peak around 1.9 Hz for L/D = 0.5, but the peak is not clear for L/D = 3 (Fig. 9b). The peak frequency, 1.9 Hz, is in a similar range to the visualized shedding frequencies of LKV, 2.2 ± 0.5 Hz. When L/D = 1, there is no clear major spectral peak because the velocity through the colony model increases with increasing L/D, and the difference between the velocity through the colony and that of detour flow decreases. Under the condition, SV and LKV are not formed clearly behind the colony model.

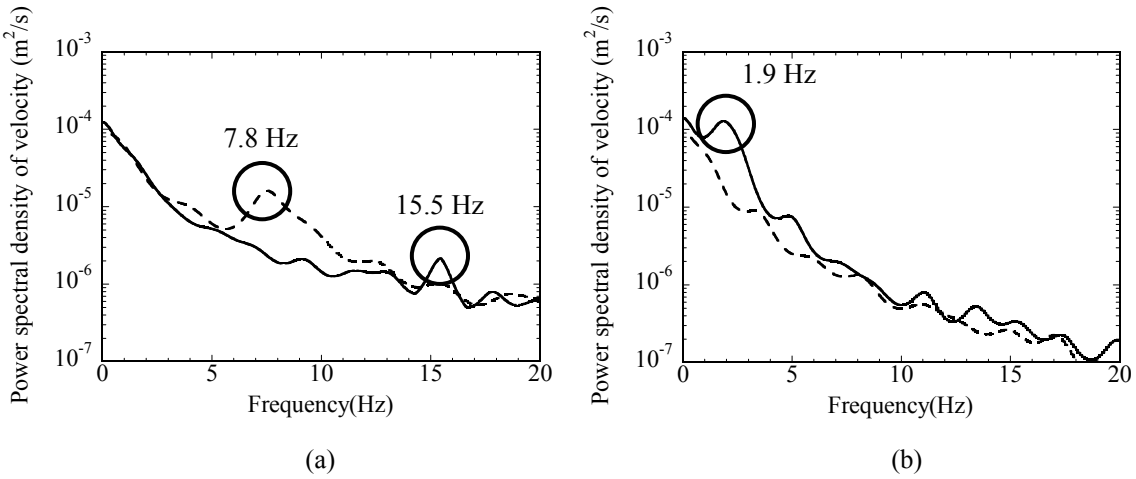

Fig. 9. Power spectral density variation with different frequencies of velocity fluctuation on *Y* direction in the wake of a colony model with a grid arrangement. *U*=0.4m/s. (a) Point A and (b) Point B; solid line, *L*/*D*=0.5; dashed line, *L*/*D*=3.

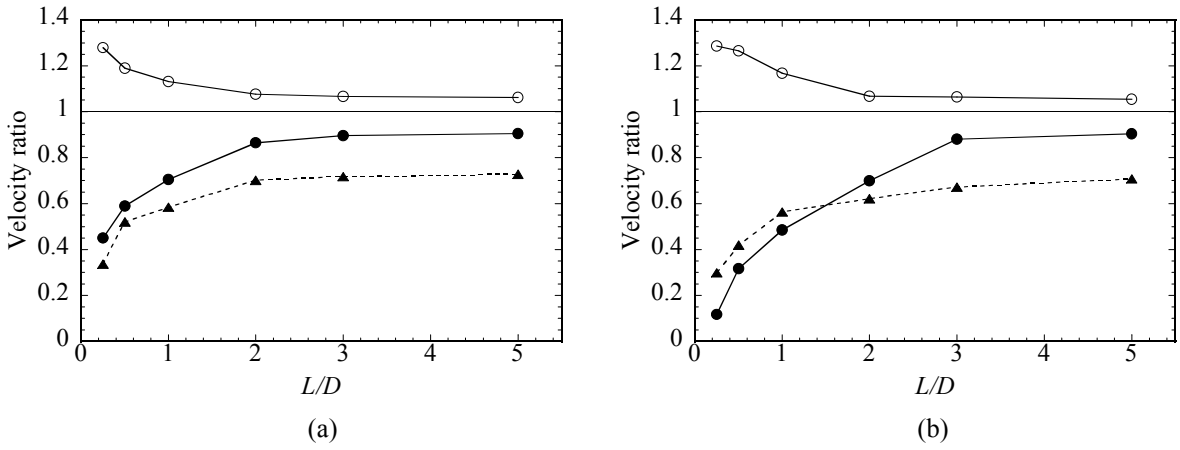

Fig. 10. The variation of three types of velocity ratios. u_{ave}/U, u_1/U and u_{detour}/U, with respect to *L*/*D*. u_{ave}: average velocity through the colony model (Y1-Y7), u_1: velocity through the colony model at Y4 for the grid pattern model or at Y6 for the staggered pattern model and u_{detour}: average velocity of detour flow at X1-X3. (a) Grid arrangement. (b) Staggered arrangement. ▲, u_{ave}/U; ●, u_1/U; ○, u_{detour}/U.

3.3. Velocity through the colony models

Three velocities around the colony model, u_{ave} (average velocity through the colony model), u_1 (average velocity through the colony model at Y4 in a grid arrangement or Y6 in a staggered arrangement) and u_{detour} (average velocity of detour flow at X1, X2 and X3) are shown as a function of *L*/*D* in Fig. 10. In the case of the grid arrangement (Fig. 10a), both u_{ave} and u_1 increase rapidly with *L*/*D* from 0.25 to 0.5, but only gradually for *L*/*D* >1. On the other hand, the detour flow velocity, u_{detour}, shows the opposite tendency. u_{detour} decreases rapidly with increasing *L*/*D* from 0.25 to 0.5, but gradually for *L*/*D* >1. In the flow visualization, the

recirculation zone behind cylinder C4 is observed clearly for L/D = 0.5. However, the zone is not formed easily for L/D >1 because then the difference between the velocity through the colony model and that of the detour flow is small. In the case of staggered arrangement (Fig. 10b), u_{ave} exhibits a similar trend to the grid arrangement, but the trend for u_1 is rather different. It increases with increasing L/D from 0.25 to 3. The velocity difference in both arrangements is caused by the difference of G/D even for the same L/D.

3.4. Drag forces on the colony models

The relationship between the drag force on the colony model and L/D is shown in Fig. 11(a). The drag force value has a different increasing tendency in the two arrangements. Bokaian and Geoola (1984) reported that C_{ds} of a backside cylinder were smaller than that of the front and recovered about 98% of C_{ds} on the front cylinder in the distance of L/D > 20 when the two cylinders were arranged in a streamwise direction. In the staggered arrangement, on the other hand, C_{ds} of the backside cylinder took about 98% value even at the close distance of L/D = 1. The spacing between cylinders in the longitudinal direction (i.e., A1 and A5, S1 and S3) is different in both arrangements even if L/D is same, and this difference is supposed to affect the increasing tendency of drag force. Moreover, the largeness of frontal projection area in the staggered arrangement is one reason for the difference in drag force.

The drag coefficient on the colony model varies with L/D, as shown in Fig. 11(b). In the grid arrangement, C_{dc} is around 1 when L/D = 0.25, close to that of a single cylinder. C_{dc} increases with L/D but becomes almost invariant around 1.3 when L/D > 1. On the other hand, C_{dc} of the colony model with a staggered arrangement decreases around 10% with increasing L/D from 0.25 to 1. In this range, the backside cylinders are sheltered by the front-side cylinders (i.e., S1 and S4); hence, the frontal projection area increases with L/D. This causes C_{dc} of the colony model with a staggered arrangement to decrease in spite of the increase in drag force. Moreover, the gap, G (see Fig. 2), also vanishes due to the overlap of the cylinders when L/D <1. Therefore, when L/D >1, the G/D increases with L/D. In this range, C_{dc} of the colony model with staggered arrangement increases slightly with L/D until it attains almost the same value as the grid arrangement case.

To understand the C_{dc} trend for the colony model, the variations of C_{ds} for cylinders A1-A5 with L/D are investigated (Fig. 12). C_{ds} of an individual cylinder increases with L/D from 0.5 to 1 except for A1 cylinder. C_{ds} of A1 decreases when L/D increases from 0.5 to 1. There is a significant difference in C_{ds} (around 40%) between A1 and A2 when L/D = 1. The difference decreases with increasing L/D because the detour flow around A1 does not have much effect on A2, although the difference still remains around 10 % when L/D = 3. The change of drag coefficient by the interaction between front-side two cylinders (L1 and L2 in Fig. 1c when α=45°) as a function of L/D was also confirmed by Lam *et al.* (2003a). Thus, the flow velocity through the colony model depends on the distance between A1 and A2. An increasing trend of C_{ds} is noted in the cases of A4 and A5 when L/D increases from 0.5 to 3 because the velocity through the colony model increases with L/D.

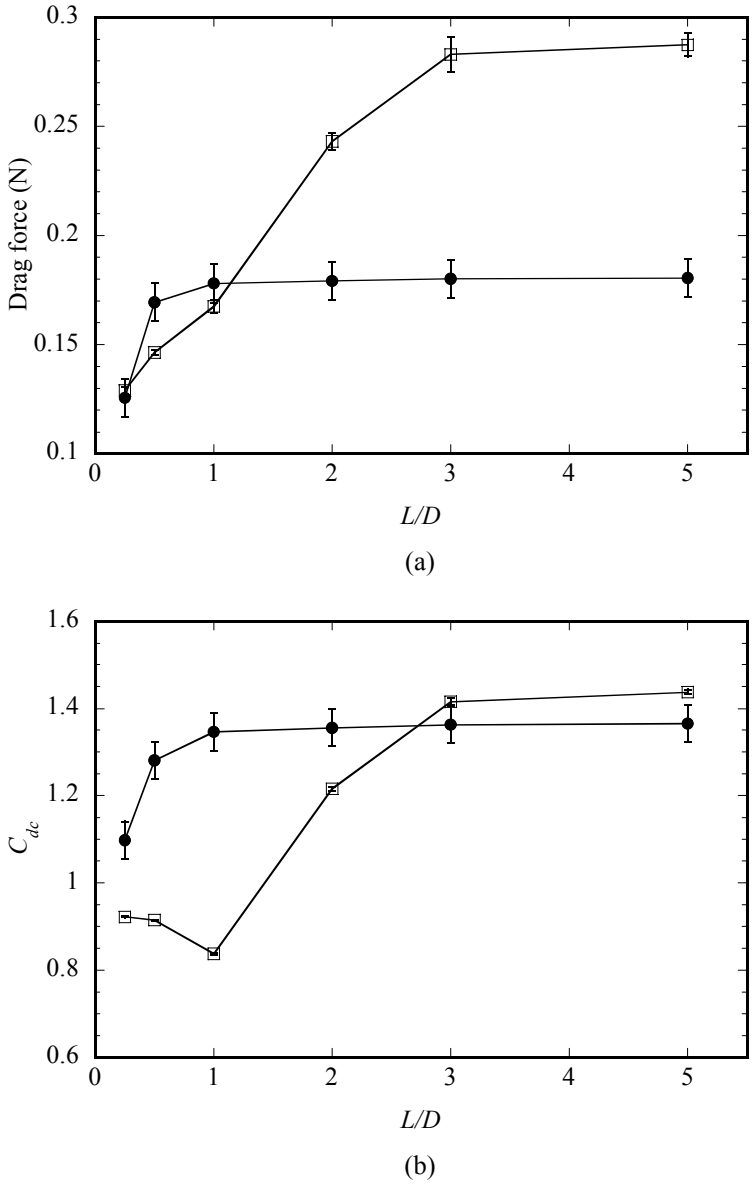

Fig. 11. Relationship between L/D and drag force or C_{dc} for colony models (with a grid arrangement or a staggered arrangement). Approach velocity U is 0.4 m/s. The error bar indicates standard deviation. (a) Drag force, (b) C_{dc}; ●, grid arrangement; □, staggered arrangement.

C_{ds} of A3 has a peak value at L/D =2. With increasing L/D, the velocity passing through the colony model increases and affects A3 cylinder, and C_{ds} of A3 cylinder increases until L/D =2. C_{ds} of A3 cylinder decreases slightly from L/D =2 to L/D = 3 because the detour flow by cylinder A1 passes between A3 and A4.

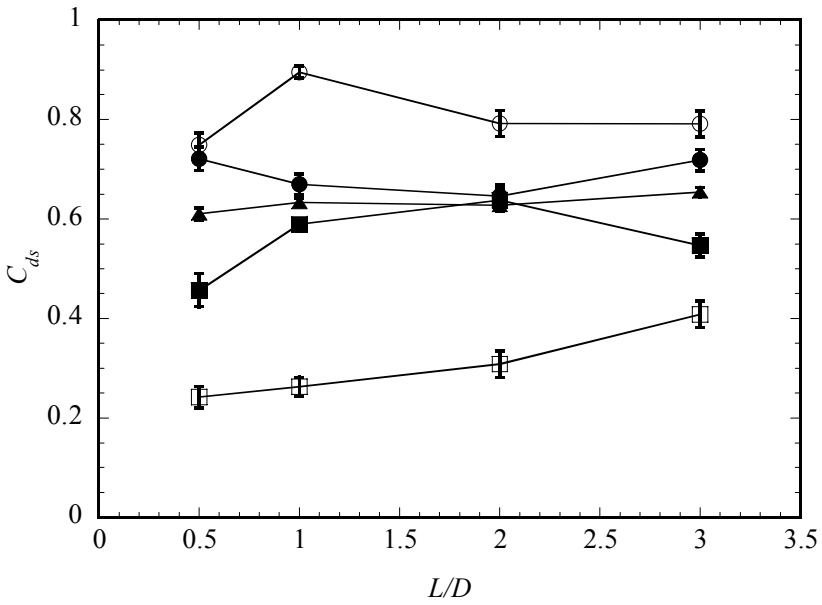

Fig. 12. Relationship between L/D and C_{ds} for individual cylinders in the colony model with a grid arrangement. Approach velocity U is 0.4 m/s. The error bar indicates standard deviation; ●, A1; ○, A2; ■, A3; □, A4; ▲, A5.

4. Discussion

4.1. Global instability of shedding vortices behind colony model

The change of flow structures around colony model is discussed here with respect to L/D, G/D, arrangement and the instabilities of vortex streets. Bearman (1967) reported by experiments that the Strouhal number, based on the vortex shedding frequency, the flow velocity at the separation point just outside the boundary layer on a circular cylinder and the lateral displacement between the vortex rows, is close to 0.18. The largeness of S_{tg} compared with S_{tsh} for $L/D = 0.5$ (Fig. 8) indicates that the spacing between the vortices is narrower than that of the stable condition of Bearman (1967). Consequently, a similar flow structure forms around a circular cylinder, a large separation bubble behind the colony model, the small vortices along the separation bubble and LKV shedding to the downstream. The Strouhal number S_{tsh} in LKV is close to the value investigated by Bearman (1967) if we use u_1 as a reference velocity of S_{tsh}. The different Strouhal numbers between S_{tg} and S_{tsh} and reconfiguration of vortices were also observed behind a group of circular cylinders (Sayers, 1990), in the vortex street from a sphere in uniform flow (Sakamoto and Haniu, 1990) and in flow structures behind a hemisphere located on a plate (Tamai *et al.*, 1987), although the vortex structures were different in each bluff body. In addition, two cylinders (Kim and Durbin, 1988; Sumner *et al.*, 1999; Akilli *et al.*, 2004) and three cylinders (Sumner *et al.*, 1999; Akilli *et al.*, 2004) arranged side-by-side in a steady cross-flow also produce such

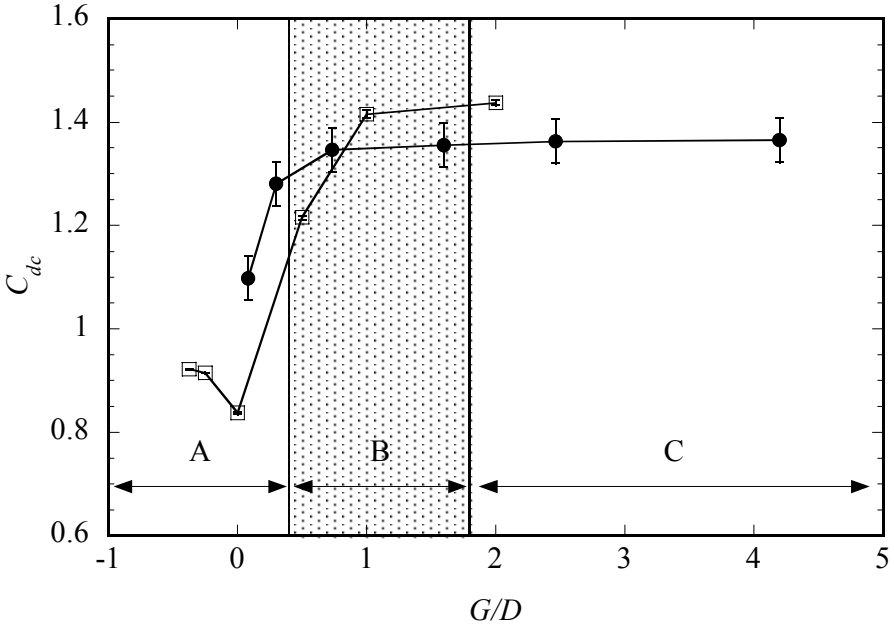

Fig. 13. Relationship between G/D and C_{dc} for the colony model. Here, A and C indicate the range of G/D where a LKV behind the colony model and a PKV from individual cylinders can be observed, respectively. B is defined as the transition zone of the two flow structures. ●, grid arrangement; □, staggered arrangement.

complex structures as small-scale vortices and LKV. The ratio S_{tg} / S_{tsh} for L/D = 0.5 ranges between about 2.2 ~ 2.7, and these values are similar to those of the cylinder and hemisphere in Fig. 8. The ratio S_{tg}/ S_{tsh} in previous studies ranged between 2.5 ~ 4 (Sumner *et al.*, 1999), 1.3 ~ 3 (Akilli *et al.*, 2004) for the flow behind two cylinders, and 3.2 ~ 4.3 (Sumner *et al.*, 1999) behind three cylinders, depending on L/D or G/D. Our S_{tg} in the grid arrangement is smaller than that in the staggered arrangement for L/D = 0.5, and S_{tg} in both arrangements decreases with L/D from 0.5 to 1 for fixed values of Re (Fig.8). These are caused by the difference in the velocity between the flow through the colony model and the detour flow, which decreases with increasing L/D (Fig.10). Moreover, S_{tg} for the grid arrangement with L/D = 3 is close to the value observed by Bearman (1967), and PKV can exist stably.

4.2. Effect of cylinder arrangement on flow structures around colony model

In this section, the effects of different arrangements of cylinders on the flow structures are discussed with the change of L/D and the velocities around the colony model as shown in Fig. 10. The non-dimensional velocity u_1/U through the colony model increases rapidly at first and then gradually with L/D in the both arrangements. The velocity ratio u_1/U increases until L/D =2 and 3, for grid and staggered arrangements, respectively. LKV is formed in the range where u_1/U increases greatly. Moreover, u_1/U for the staggered arrangement is smaller than that for the grid arrangement when L/D is less than 3. Because, the values of G/D in the grid and staggered arrangements are quite different, i.e. 0.7 and 0, respectively, for L/D =1. It

means that the blocking effect is quite different for the two arrangements, even when the L/D is the same. As a result, LKV is generated when L/D =1 with the staggered arrangement because of the large velocity difference between the flow through the colony model and the detour flow.

4.3. Variation of the drag coefficient C_{dc} for the colony model and flow structures with G/D

The results in section 4.2 indicate that L/D is not always a useful parameter for the flow structures around the colony model. Then, C_{dc} of the colony model and the flow structure are rearranged using G/D (Fig.13) because it affects the stability of PKV. The generation of LKV is occurred for G/D <0.4 (L/D < 0.5 and L/D < 1 in the grid and staggered arrangements, respectively). PKV is clearly formed behind individual cylinders in the colony model in the range of G/D >1.8 (L/D >3 and L/D >5 in the grid and staggered arrangements, respectively), where C_{dc} of the colony model is little changed because of the small velocity difference between the flow through the colony model and the detour flow. In previous research, the effect of cylinder arrangements on the flow around two or three cylinders arranged side-by-side was also reported as negligible at G/D >1.5 (Sumner *et al.*, 1999; Akilli *et al.*, 2004). However, in this study, the threshold of G/D is assumed about 1.8 because of the difference in arrangement and number of cylinders. The range of $0.4<G/D<1.8$ can be defined as a transition region. In the transition region, the velocity through the colony model increases with G/D; however, PKV is not formed stably because the spaces G/D are smaller than the length for the stable length for two row vortices. The changing point of the C_{dc} curve is located in the middle of this region. Thus, the vortex structures behind the colony model and the trend of C_{dc} are well represented by G/D.

5. Summary

The fluid force on colony-type vegetation and the flow structure around it were investigated experimentally in a water flume. It was found that the change in large-scale and small-scale vortex structures is related to the interaction and the instability of a primitive Kármán vortex street behind each cylinder. The gap spacing G on cross-stream direction has an important role for the variation in case of our proposed colony model. Further study is required by changing the ratio of colony scale (D_c)/ small scale (D) to consider the similarity and apply C_d to natural environment. In addition it is quite important to investigate the transition region and the effects of the interaction between a horseshoe vortex and a Kármán vortex street on the drag coefficient with changing hydraulic conditions and G/D of the colony.

Acknowledgements

We thank Mr. Yagisawa for his help in experiments and the referees for helpful suggestions. The research was partially funded by a JSPS Grant-in-Aid for Scientific Research (No. 17560452).

References

Akilli, H, Akar, A. and Karakus, C. 2004. Flow characteristics of circular cylinders arranged side-by-side in shallow water, Flow Measurement and Instrumentation, 15, 187-197.
Baker, C. J. 1980. The turbulent horseshoe vortex, J. Wind Eng. Ind. Aerodyn., 6, 9-23.
Bearman, P. W. 1967. On vortex street wakes, J. Fluid Mech., 28, 625-641.
Bokaian, A. and Geoola, F. 1984. Wake-induced galloping of two interfering circular cylinders, J. Fluid Mech., 146, 383-415.
Castro, I. P. 1971. Wake characteristics of two-dimensional perforated plates normal to an air-stream, J. Fluid Mech., 46(3), 599-609.
Choi, S. and Kang, H. 2004. Reynolds stress modeling of vegetated open-channel flows, J. Hydraulic Research, 42(1), 3-11.
Dalton, C. and Szabo, J. M. 1977. Drag on a group of cylinders, Trans. ASME J. Pressure Vessel Tech., 99, 152-157.
Helmiö, T. 2002. Unsteady 1D flow model of compound channel with vegetated floodplanins, J. Hydrology, 269, 89-99.
Järvelä, J. 2002. Flow resistance of flexible and stiff vegetation: a flume study with natural plants, J. Hydrology, 269, 44-54.
Kim, H. J. and Durbin, P. A. 1988. Investigation of the flow between a pair of circular cylinders in the flopping regime, J. Fluid Mech., 196, 431-448.
Kiya, M., Arie, M., Tamura, H. and Mori, H. 1980. Vortex shedding from two circular cylinders in staggered arrangement, Trans. ASME J. Fluid Eng., 102, 166-173.
Kouwen, N., Li, R. M. and Simons, D. B. 1981. Flow resistance in vegetated waterways, Trans. ASAE, 24(3), 684-698.
Lam, K., Li, J. Y., Chan, K. T. and So, R. M. C. 2003a. Flow pattern and velocity field distribution of cross-flow around four cylinders in a square configuration at a low Reynolds number, J. Fluids and Structures, 17, 665-679.
Lam, K., Li, J. Y. and So, R. M. C. 2003b. Force coefficients and Strouhal numbers of four cylinders in cross flow, J. Fluids and Structures, 18, 305-324.
Li, R. and Shen, H. 1973. Effect of tall vegetations on flow and sediment, J. Hydraulics Division, ASCE, 97, HY5, 793-814.
Melville, B. W. and Sutherland, A. J. 1988. Design method for local scour at bridge piers, J. Hydr. Engrg., ASCE, 114, 1210-1226.
Musick, H. B., Trujillo, S. M. and Truman, C. R. 1996. Wind-tunnel modelling of the influence of vegetation structure on saltation threshold, Earth Surf. Processes Landf., 21, 589-605.
Nepf, H. M. 1999. Drag, turbulence, and diffusion in flow through emergent vegetation, Water Resour. Res., 35(2), 479-489.
Okamoto, S., Satoh, I., Shiina, M. and Tamura, M. 1994. Effect of spacing between two adjoining circular cylinders on flow around two-dimensional circular cylinder rows (2nd report, two and three rows of transverse arrangement), Trans. JSME, 60(573), 48-54.
Okamoto, S. and Sunabashiri, Y. 1992. Vortex shedding from a circular cylinder of finite

length placed on a ground plane, Trans. ASME J. Fluid Eng., 114, 512-521.
Okamoto, T. and Yagita, M. 1973. The experimental investigation on the flow past a circular cylinder of finite length placed normal on the plane surface, Bulletin of the JSME, 16(95), 805-814.
Righetti, M. and Armanini, A. 2002. Flow resistance in open channel flows with sparsely distributed bushes, J. Hydrology, 269, 55-64.
Sakamoto, H. and Haniu, H. 1990. A study on vortex shedding from spheres in a uniform flow, Trans. ASME, 112, 386-392.
Sayers, A. T. 1990. Vortex shedding from groups of three and four equispaced cylinders situated in a cross flow, J. Wind Eng. and Industrial Aerodynamics, 34, 213-221.
Smith, R. J., Hancock, N. H. and Ruffini, J. L. 1990. Flood flow through tall vegetation, Agric. Water Manage., 19, 317-332.
Struve, J., Falconer, R. A. and Wu, Y. 2003. Influence of model mangrove trees on the hydrodynamics in a flume, Estuarine, Coastal and Shelf Science, 58, 163-171.
Sumner, D., Wong, S. S. T., Price, S. J. and Païdoussis, M. P. 1999. Fluid behaviour of side-by-side circular cylinders in steady cross-flow, J. Fluids and Structures, 13, 309-338.
Tamai, N., Asaeda, T. and Tanaka, N. 1987. Vortex structures around a hemispheric hump, Boundary-Layer Meteorol., 39, 301-314.
Tatsuno, M., Amamoto, H. and Ishi-i, K. 1991. On the stable posture of a pair of parallel cylinders in a uniform flow, Fluid Dyn. Res., 8, 253-272.
Tatsuno, M., Amamoto, H. and Ishi-i, K. 1998. Effects of interference among three equidistantly arranged cylinders in a uniform flow, Fluid Dyn. Res., 22, 297-315.
Thompson, G. T. and Roberson, J. A. 1976. A theory of flow resistance for vegetated channels, Trans. ASAE, 288-293.
Zdravkovich, M. M. 1977. Review of flow interference between two circular cylinders in various arrangements, Trans. ASME J. Fluid Eng., 99, 618-633.